SIMULATING THE USE OF UAV PHOTOGRAMMETRY FOR MONITORING LAND SUBSIDENCE AT URBAN AREA

Dimas C Alamsyah

Geodesy Research Group, Faculty of Earth Sciences and Technology, Institut Teknologi Bandung, Jl. Ganesha 10, Bandung, Indonesia
Email: dimascandika@gmail.com

Abstract

The Unmanned Aerial Vehicle (UAV) photogrammetry method has been widely used in various applications. One of the potential photogrammetry methods is to estimate the land deformation, e.g., land subsidence. This study aims to analyze the opportunity of UAV photogrammetry utilization for detecting the land subsidence urban areas, including relatively low cost and wide area coverage in a relatively short time. Two photogrammetry measurements were conducted in two different epochs with different flight altitudes to analyze the potential use of the photogrammetry method. The Digital Surface Model (DSM) generated from two different observation periods will be compared to obtain a land subsidence model. Based on the result, the photogrammetry method can detect land subsidence if a minimum subsidence value of 5 cm exists for an altitude flight height of 80 meters, 10 cm for an altitude flight height of 100 meters, and 11 cm for an altitude flight height of 150 meters. We also highlight several things to consider when applying the photogrammetry method to observe land subsidence, e.g., remove the uncorrelated height values obtained from different observations.

Keywords: UAV, DSM, land subsidence monitoring.

Introduction

Photogrammetry is a mapping method that is currently widely used. The advantage of the photogrammetry method compared to other methods such as Global Navigation Satellite System (GNSS) observations is its ability to map large areas at a fairly low cost [1]. The platform generally used in the photogrammetry method is the aircraft, but over time, it is starting to be replaced with the Unmanned Aerial Vehicle (UAV) or what we know as drones. UAV photogrammetry can be considered as the latest photogrammetry measurement tool [2].

The drone is then massively used and developed for mapping needs, but the common camera used on the drone is a non-metric camera[3]. The non-metric camera is not specifically designed for mapping purposes, so the resulting accuracy is may not as good as metric cameras. The solution to this problem is calibrating the camera before data

acquisition (precalibrated). This is done to reduce systematic errors such as the bowl effect that will affect Digital Elevation Model (DTM) [4].

The utilization of the UAV photogrammetry method does not stop only for mapping needs[5]. One of the other potentials used of the UAV photogrammetry method is to evaluate the surface changes, e.g., land subsidence, by comparing two different digital surface models (DSMs) obtained at different acquisition times[6]. Land subsidence itself explains the changes in the geometric shape of objects horizontally and vertically from the initial conditions, from the point of view of time [7].

Land subsidence is one of the problems that cause potential disasters. One of the problems caused by land subsidence is flooding. The cause of the subsidence is thought to be due to excessive groundwater exploitation [8]. As subsidence occurs in a relatively big area, several geodetic methods, such as leveling and GNSS observations, are time-consuming[9]. So it is very important to assess the applicability of the photogrammetric method for sensing land surface deformation, as it offers time and cost-efficiency[10]. In this study, the UAV photogrammetry method will be tested to analyze the method's applicability.
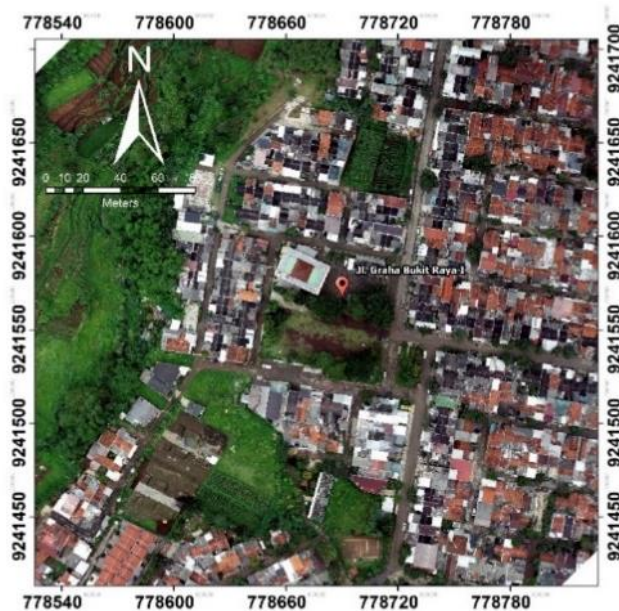

Figure 1
Research area

The research was simulated in a residential area with a research area coverage as visualized in Figure 1. Particularly for this simulation, we focus on an area covering 5 hectares that are currently carrying out the dredging and stockpiling process for other residential development needs. This location was deliberately chosen because it is

considered suitable for testing this method. After all, the surface changes that occur can be observed quickly, and the changes obtained are quite significant, as evidenced by the visualization of the area in Figure 2. Additionally, mapping the area in a wider area was intended to place the Ground Control Point (GCP) and independent Check Point (ICP) freely with a fairly even distribution.
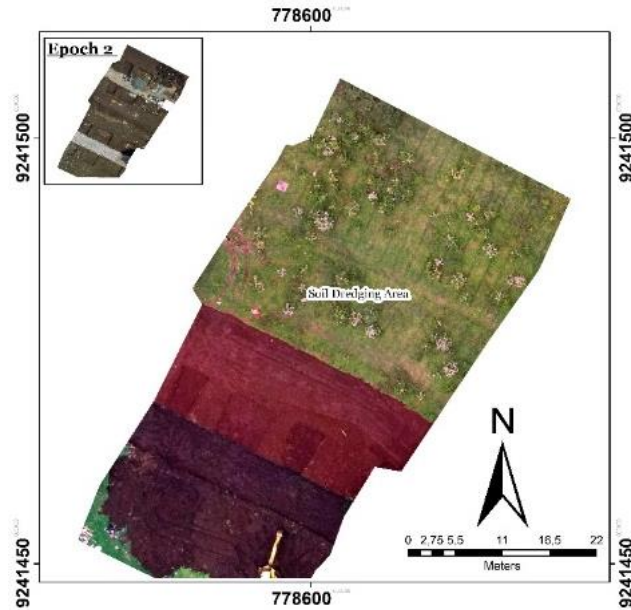

Figure 2
Dredging area visualization

METHODOLOGY

In the acquisition process, photogrammetry was conducted at different flight heights and two different epochs[11]. The time interval of data collection for the first (T1) and second (T2) data acquisitions is one month, where the research area changed due to dredging. Details of the planning of the acquisition process can be seen in Tabel 1.

Tabel 1
Data acquisition parameters

Data Acquisition Parameters	
Mission Code	Flying Altitude (m)
Mission 1 (T1)	80
Mission 2 (T1)	100
Mission 3 (T1)	150
Mission 4 (T2)	80
Mission 5 (T2)	100
Mission 6 (T2)	150

The data acquisition process began with the installation of GCPs and ICPs, then continued with acquiring coordinate values using GNSS with the Real-Time Kinematic (RTK) method, then proceeded with the acquisition of aerial photos. The GCPs and ICPs installation location is visualized in Figure 3.

From the data that has been acquired, data processing is carried out. Data processing in the UAV photogrammetry processing starts from the image matching process, then continues with the resection and intersection process, only after that forms a DEM and proceeds to the orthomosaic map formation stage. In this study, the Digital Surface Model (DSM), a derivative product of DEM, is used to analyze altitude information, while orthomosaic map was chosen to help visualize the changes that occur in areas experiencing land subsidence.
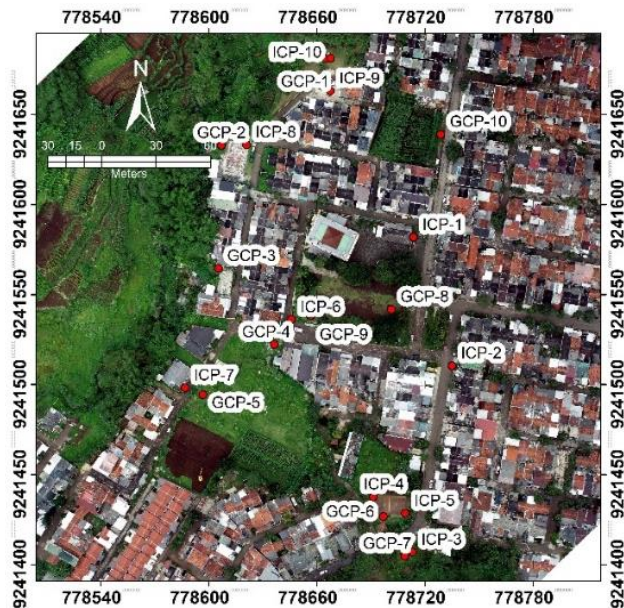

Figure 3
Distribution of GCPs and ICPs

The acquisition results at two epochs with different flight altitude variations are processed to obtain DSMs. The DSMs from the processing result are then paired according to the flight variation. Then, we formed layer data of 2500 by 2500 points to form a dense grid. We can see the point visualization in Figure 4.

Figure 4
Visualization of gridded sample data

The point layer data for each pair of altitude height variations are then filled in with the height value from the DSM of each model formed from each epoch. The height data is compared and cleaned of existing errors assisted using regression analysis and statistical distributions. The height data that has been cleaned of the error value is then set aside and used as data to form a land subsidence model using the kriging interpolation model. The data processing flow can be seen in Figure 5.
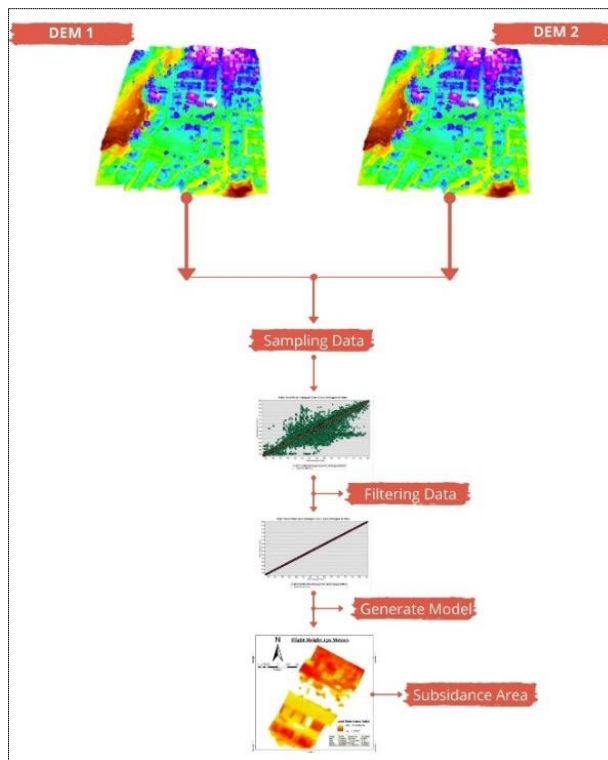

Figure 5
Data processing diagram

2.1 MEASUREMENT OF GROUND CONTROL POINT (GCP) AND INDEPENDENT CHECK POINT (ICP)

Ground Control Points (GCPs) are required for constraining data point clouds[12]. The results of the basic processing of aerial photos can later be corrected for the coordinate values into the coordinate values of the ground to represent the actual position. Independent Checkpoints (ICPs) are intended to check the accuracy value of the formed model and tied to the ground control point. The horizontal GNSS position accuracy value is denoted by Root mean square Horizontal (RMSH), while vertical GNSS position accuracy is denoted by Root mean square Vertical (RMSV)[13]. Tabel 2 and Tabel 3 show the coordinates for GCP and ICP at two different epochs.

The coordinates of the GCPs and ICPs were estimated by using the Hemisphere GNSS receiver. The RTK method was implemented and tied to the Continuously Operating Reference Stations (CORS) belonging to the Geospatial Information Agency with the codename of CLBG in the Lembang area, with a baseline length about 10 to 11 kilometers to the measurement location. The correction was given using the Networked Transport of RTCM method via Internet Protocol (NTRIP).

Tabel 2
GCP and ICP coordinates one for epoch

GCP and ICP First Data Acquisition (UTM Zone 48 S)					
Point	Easting (m)	Northing (m)	Elevation (m)	RMSEH (m)	RMSEV (m)
GCP-1	778664.733	9241680.998	765.493	0.006	0.014
GCP-2	778606.94	9241632.858	762.154	0.007	0.015
GCP-3	778605.236	9241564.463	761.172	0.01	0.02
GCP-4	778636.277	9241522.222	760.644	0.007	0.013
GCP-5	778596.592	9241494.368	760.899	0.006	0.011
GCP-6	778696.852	9241426.683	757.317	0.006	0.011
GCP-7	778708.783	9241404.64	756.095	0.006	0.01
GCP-8	778701.325	9241541.795	761.388	0.011	0.021
GCP-9	778656.456	9241538.098	761.43	0.006	0.012
GCP-10	778728.78	9241638.97	765.905	0.008	0.015
ICP-1	778713.62	9241581.853	762.969	0.009	0.019
ICP-2	778735.017	9241510.38	758.225	0.009	0.019
ICP-3	778712.944	9241406.955	756.073	0.009	0.019
ICP-4	778691.256	9241437.649	757.439	0.009	0.017
ICP-5	778709.021	9241428.455	757.354	0.009	0.017
ICP-6	778645.806	9241536.109	760.966	0.006	0.013
ICP-7	778586.748	9241498.234	759.656	0.009	0.018
ICP-8	778620.87	9241633.152	762.209	0.008	0.017
ICP-9	778667.406	9241663.038	764.515	0.008	0.017
ICP-10	778667.559	9241681.269	766.003	0.006	0.013

Tabel 3
GCP and ICP coordinates for epoch two

Point	Easting (m)	Northing (m)	Elevation (m)	RMSEH (m)	RMSEV (m)
GCP and ICP Second Data Acquisition (UTM Zona 48 S)					
GCP-1	778727.955	9241632.047	765.602	0.007	0.013
GCP-2	778722.063	9241538.388	760.925	0.008	0.014
GCP-3	778695.89	9241542.674	761.479	0.006	0.011
GCP-4	778663.081	9241548.823	761.423	0.007	0.012
GCP-5	778607.169	9241532.95	760.623	0.006	0.011
GCP-6	778622.051	9241510.09	762.414	0.006	0.01
GCP-7	778709.32	9241406.532	756.099	0.009	0.017
GCP-8	778694.726	9241425.882	757.264	0.006	0.01
GCP-9	778713.669	9241576.11	762.652	0.009	0.014
GCP-10	778664.334	9241680.543	765.398	0.006	0.01
ICP-1	778713.62	9241581.853	762.969	0.009	0.019
ICP-2	778735.017	9241510.38	758.225	0.009	0.019
ICP-3	778712.944	9241406.955	756.073	0.009	0.019
ICP-4	778691.256	9241437.649	757.439	0.009	0.017
ICP-5	778709.021	9241428.455	757.354	0.009	0.017
ICP-6	778645.806	9241536.109	760.966	0.006	0.013
ICP-7	778586.748	9241498.234	759.656	0.009	0.018
ICP-8	778620.87	9241633.152	762.209	0.008	0.017
ICP-9	778667.406	9241663.038	764.515	0.008	0.017
ICP-10	778667.559	9241681.269	766.003	0.006	0.013

2.2 AERIAL PHOTO DATA PROCESSING
2.2.1 EXPORT DATA

The aerial photoshoot area produced navigational coordinates and a JPG image storage format[14]. The photoshoot of the study area includes all objects in the study area, such as trees, roads, buildings, and other objects contained in the images obtained from the shooting. The number of photos for each flying altitude is given in Tabel 4. The greater the altitude height, the fewer photos that we obtain.

The difference in the number of photos produced in the aerial photo data acquisition process which caused by adjustments to other flight parameters such as sidelap, overlap, and focal length[15]. Sidelap and overlap were closely related to the focal length and flight altitude of the vehicle because the focal length and flight altitude of the vehicle were parameters that regulate the sweep of the vehicle. Moreover, sidelap and overlap were the parameters set by the users[16]. So that, the number of photos in the acquisition process will certainly be adjusted in such a way as to get the input parameters that have been planned before.

Tabel 4
Number of Photos Based on Flying Height

Number of Photos Based on Flying Height	
Flying Altitude	Number of Photos
80	114
100	82
150	42

2.2.2 DATA IMPORT AND ELEVATION POINT ESTABLISHMENT (DENSE CLOUD)

The exported data was introduced to the Agisoft Metashape software at this stage. After the data was introduced, the data will automatically be processed based on the alignment of objects from 2 or more photos to generate sparse cloud object points and paired according to identical objects [17] as visualized in Figure 6.
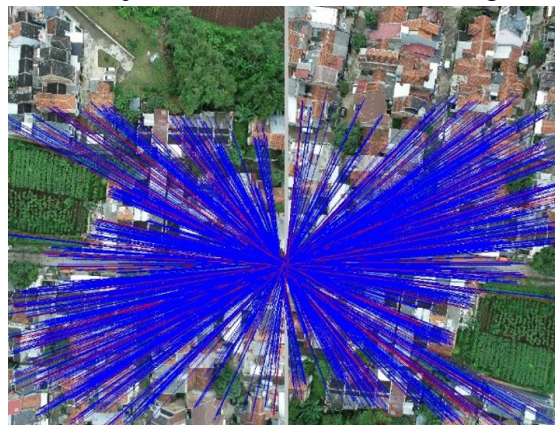

Figure 6
The illustration of formation sparse cloud process by aligning with 2 photos

The next process was to register the GCPs by matching the coordinate value with a predetermined object (premark)[18], as shown in Figure 7, to get the corrected sparse cloud.
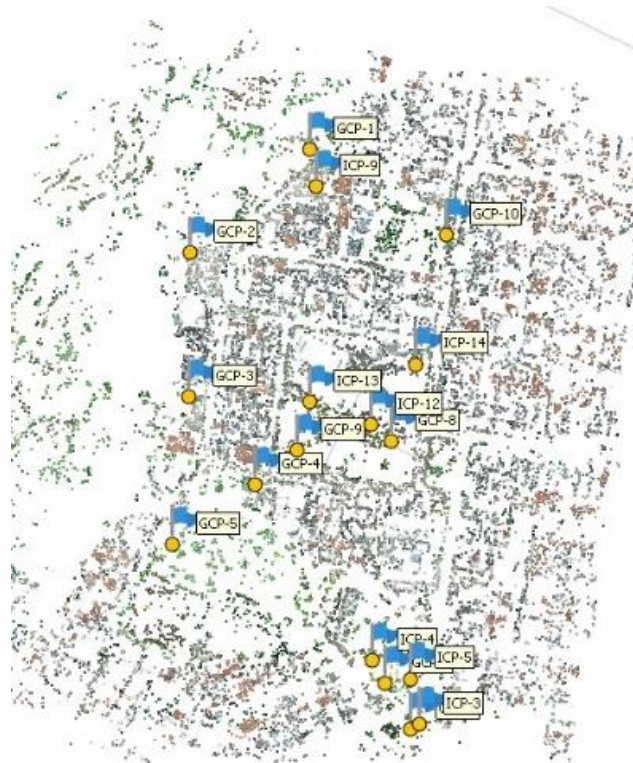

Figure 7
Result of sparse cloud that has been corrected Visualization of gridded sample data

The sparse corrected cloud then would be made into the dense cloud, which becomes a point distribution with a height value visualized by Figure 8. Those points then used to be formed of DSM.

Figure 8
Result of dense cloud formation

2.2.3 FORMATION OF THE DIGITAL SURFACE MODEL (DSM)

The formation of the DSM is an advanced process. In this research activity, DSM was formed from elevation data in the form of points called dense clouds [19]. DSM is the basic data that will be analyzed in this study. The DSM model used in this study consists of six models that can be divided into three models at a time. One of the DTM models used in the analysis process is visualized in Figure 9. The models are then analyzed according to the flight altitude parameter at the acquisition time. DSM data that has been grouped based on the data acquisition process was analyzed to determine the changes that occur between the first and second time based on altitude changes.
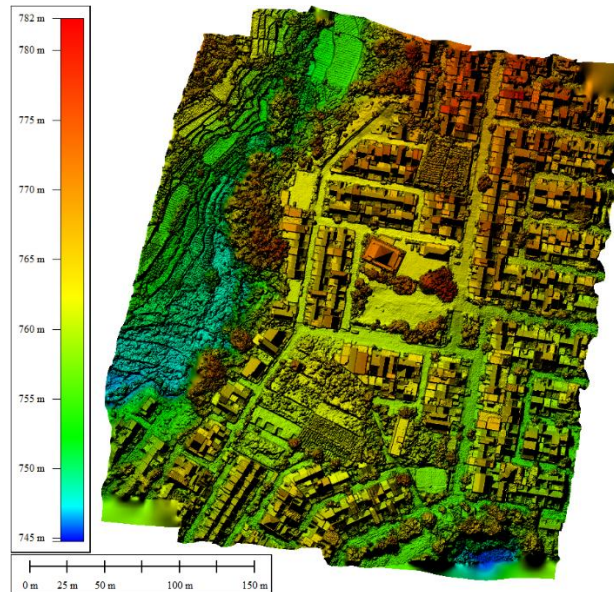
Figure 9
Results of the formation of DSM

2.3 Filtering Digital Terrain Model (DTM)

In this process, the filtering process was carried out from two DTMs with the same flight altitude, this process used sample data from both DTMs with different measurement times[20]. This was done to eliminate large errors that exist in the data caused by the movement of objects other than the ground and differences in a light hue. Sampling was done by forming a dense grid of points as visualized in Figure 4. The filtering process was assisted by a data trend graph in the visualization Figure 10 which stated the distribution of data and relative precision values between two models. The data trend graph was also used to detect errors in the comparison process between the two models.

Error visualized with a point away from the line trend formed from Figure 10, which eliminated iteratively based on the help of statistical graphs to form a graph trend which can be seen visually in Figure 11. The error range, in this case, was distinguished based on a statistical distribution divided into 256 ranges to classify errors that were accepted or must be eliminated on objects other than soil.
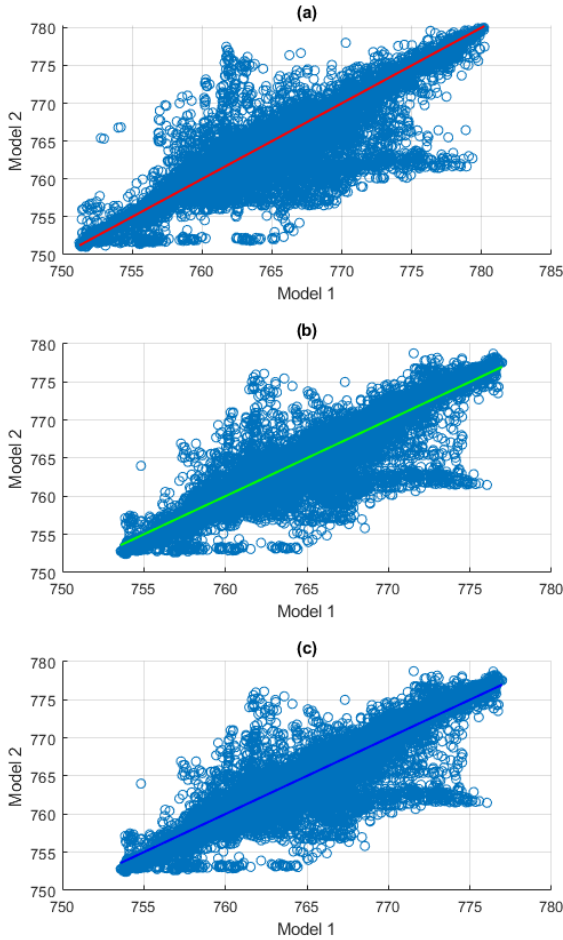
Figure 10
Visualization of model comparison trend graphs, Flight height of 80 (a),
Flight height of 100 (b), and Flight height of 150 (c) (X Axis : Model 1 Z
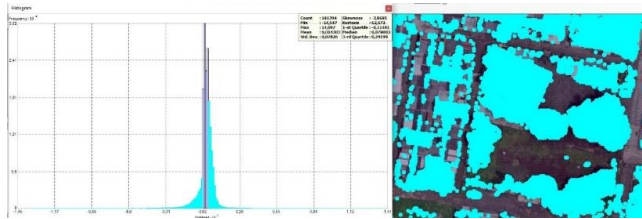**value and Y Axis : Model 2 Z Value)**

Figure 11
Visualization of the marking (right) and elimination process error based on
statistical data (left)

After eliminating, re-checking the trend graph such as the visualization in Figure 12 to confirm before proceeding to the next step, further analysis could be carried out if the trend graph was not far from the existing population value, as shown in Figure 12.
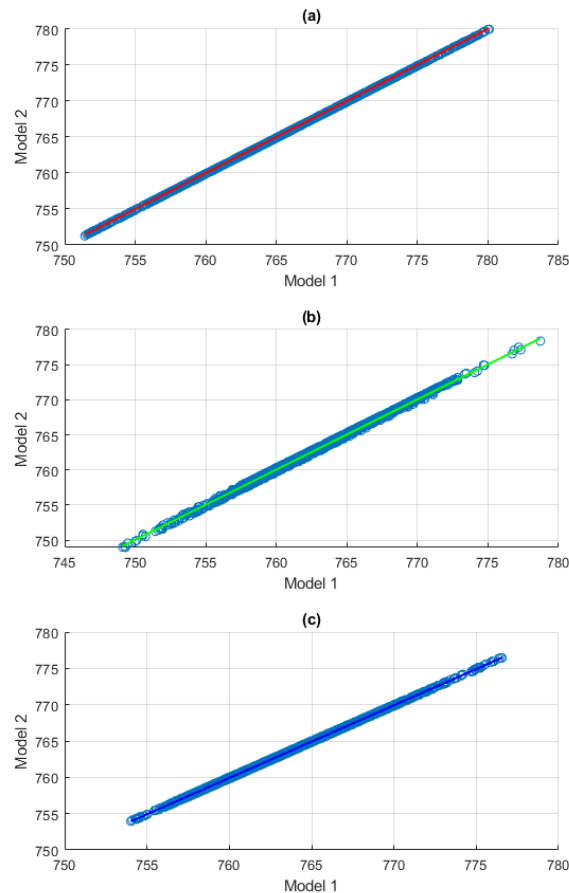

Figure 12
Trend chart visualization after filtering process, Flight height of 80 (a),
Flight height of 100 (b), and Flight height of 150 (c) (X Axis : Z value Model
1 and Y Axis : Z Value Model 2)

At this stage, the existing errors can be grouped based on visually visible data groups. The errors can be grouped based on the sources. Meanwhile, the objects that contain many errors are buildings, trees, and meadows. The error was caused by several factors, for example in the error of the building object caused by the difference in hue color between the first and second data collection and the reflection of light that was too hot, causing the formation of an increased height value on the object, then tree errors were identified due to the movement of the position of the branch and twigs so that it makes a difference of height was quite significant between two models. Besides that, errors in the fields were also identified due to the movement of objects by wind gusts. In addition, there were eliminated errors that can be tolerated. On the other side, some

mistakes usually contain the desired subsidence information. It usually exists on the ground object or road object.

Result and Discussion
LAND SUBSIDENCE MODEL

The subsidence model was formed based on sample points from the filtering stage. So that the model formed was free from random errors, statistics, and blunders. The formed model can be described in Figure 13-15.

The modeling was carried out using the kriging method, which is a geostatistical method used to estimate the value of a point or block as a linear combination of values around the point to be estimated, while the weighting performed in the kriging method is the variance of the minimum estimate by expanding the use of semivariogram.
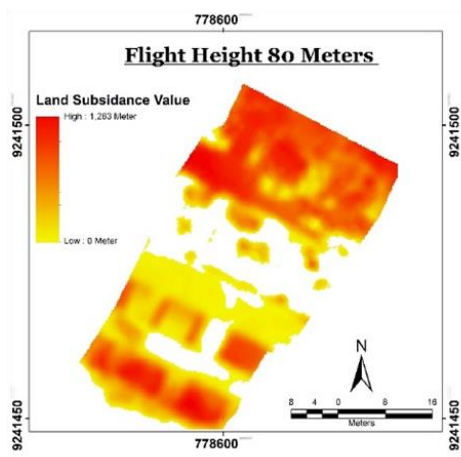

Figure 13
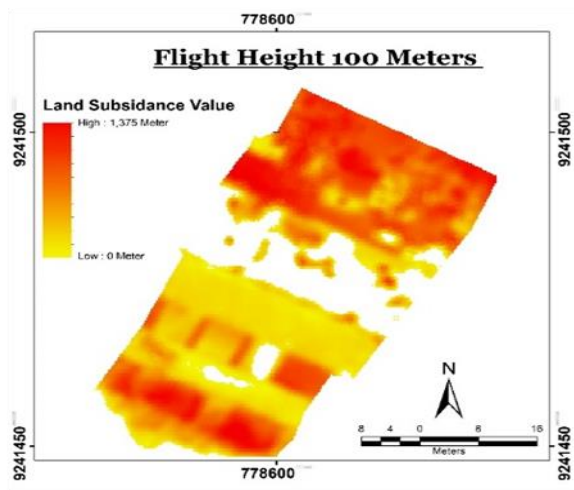**Land Subsidence Model From Photogrammetry Method With Flight Height Of 80 Meters**

Figure 14
Land Subsidence Model From Photogrammetry Method With Flight Height Of 100 Meters

Figure *15*
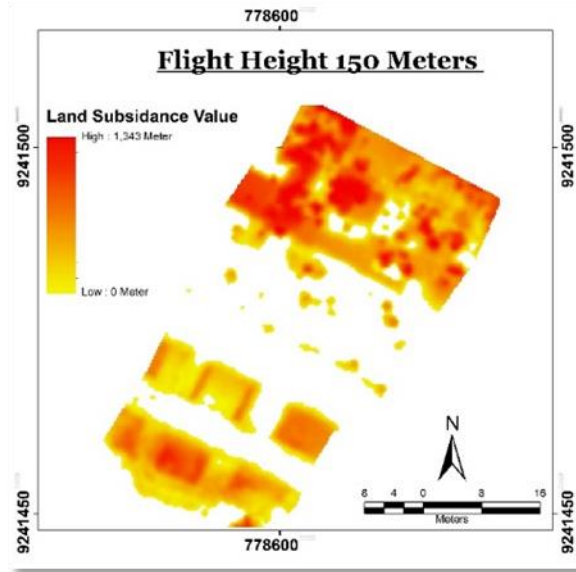**Land Subsidence Model From Photogrammetry Method With Flight Height Of 150 Meters**

3.1 LAND SUBSIDENCE MODEL VALIDATION

Validation of the land subsidence model was carried out by measuring point samples using direct measurements at locations with a large enough change value to facilitate identifying objects in the field. Data sampling was carried out in the study area, which focused on the area that was carrying out the dredging process in the first and second data collection time.
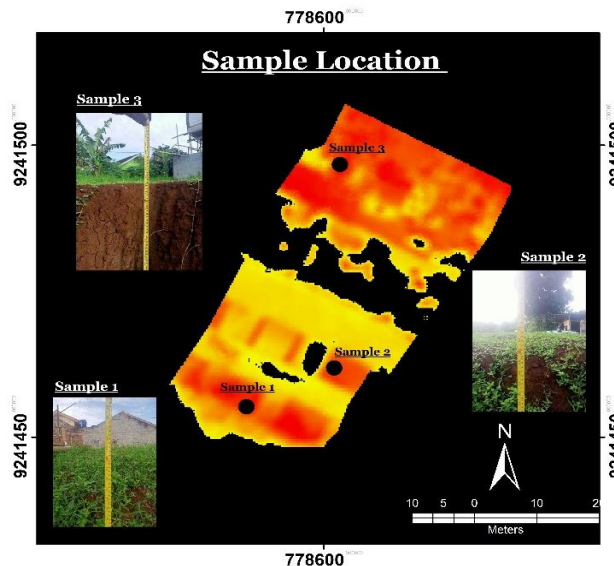

Figure *16*
Sketch of sampling point

The validation was done by performing the extraction of elevation values on the subsidence model at the validation point measured using a meter. The validation value was obtained based on the calculation of the standard deviation value from reducing the height value at the location, which can be seen in Figure 16. The value of the standard deviation of the model from this study can be seen in Tabel 5.

Tabel 4
Validation table for ground subsidence model in meters

Description	Direct Calculation	Value 80	Value 100	Value 150	Differen ce _80	Differenc e 100	Differenc e 150
Sample 3	-1.283	-1.256	-1.307	-0.977	-0.027	0.024	-0.306
Sample 2	-0.943	-0.882	-0.955	-0.663	-0.061	0.012	-0.280
Sample 1	-0.625	-0.643	-0.814	-0.519	0.018	0.189	-0.106
Sample Deviation Standards					0.040	0.099	0.109
Average					-0.023	0.075	-0.231

Conclusion

The UAV photogrammetry method was feasible to be used as a method for detecting land subsidence if a minimum subsidence value of 5 cm exists for a flight height of 80 meters, 10 cm for a flight height of 100 meters, and 11 cm for a flight height of 150 meters.

Additionally, we highlight several things to be considered when using UAV photogrammetry for subsidence monitoring applications. The acquisition in UAV photogrammetry for the needs of land subsidence monitoring analysis must use the same flight acquisition parameters, including side lap by 60%, overlap by 80%, and lowest flight altitude taking into account the proper conditions for flight. Then, error filtering was done repeatedly and always paid attention to the error trend graph and standard deviation value. So that not to eliminate the height value, which will be grouped into land subsidence values. The filtering process endeavored was not to eliminate the height value of the land object. The data modeling parameters use the same parameters.

Dimas C Alamsyah

BIBLIOGRAFI

[1] F. Franceschini, M. Galetto, D. Maisano, And L. Mastrogiacomo, "Large-Scale Dimensional Metrology (Lsdm): From Tapes And Theodolites To Multi-Sensor Systems," *Int. J. Precis. Eng. Manuf.*, Vol. 15, No. 8, Pp. 1739–1758, 2014.

[2] H. Eisenbeiß, "Uav Photogrammetry," Eth Zurich, 2009.

[3] G. Casagrande, "Opportunities," In *Small Flying Drones*, Springer, 2018, Pp. 47–89.

[4] D. Griffiths And H. Burningham, "Comparison Of Pre-And Self-Calibrated Camera Calibration Models For Uas-Derived Nadir Imagery For A Sfm Application," *Prog. Phys. Geogr. Earth Environ.*, Vol. 43, No. 2, Pp. 215–235, 2019.

[5] A. Fritz, T. Kattenborn, And B. Koch, "Uav-Based Photogrammetric Point Clouds—Tree Stem Mapping In Open Stands In Comparison To Terrestrial Laser Scanner Point Clouds," *Int. Arch. Photogramm. Remote Sens. Spat. Inf. Sci*, Vol. 40, Pp. 141–146, 2013.

[6] D. Gasperini, P. Allemand, C. Delacourt, And P. Grandjean, "Potential And Limitation Of Uav For Monitoring Subsidence In Municipal Landfills," *Int. J. Environ. Technol. Manag.*, Vol. 17, No. 1, Pp. 1–13, 2014.

[7] A. H.-M. Ng *Et Al.*, "Mapping Accumulated Mine Subsidence Using Small Stack Of Sar Differential Interferograms In The Southern Coalfield Of New South Wales, Australia," *Eng. Geol.*, Vol. 115, No. 1–2, Pp. 1–15, 2010.

[8] H. Z. Abidin, H. Andreas, I. Gumilar, And Y. Fukuda, "E. Pohan, Ye, Deguchi, T.(2011), Land Subsidence Of Jakarta (Indonesia) And Its Relation With Urban Development," *Nat.Hazards*.

[9] M. Shirzaei, J. Freymueller, T. E. Törnqvist, D. L. Galloway, T. Dura, And P. S. J. Minderhoud, "Measuring, Modelling And Projecting Coastal Land Subsidence," *Nat. Rev. Earth \& Environ.*, Vol. 2, No. 1, Pp. 40–58, 2021.

[10] N. An *Et Al.*, "Plant High-Throughput Phenotyping Using Photogrammetry And Imaging Techniques To Measure Leaf Length And Rosette Area," *Comput. Electron. Agric.*, Vol. 127, Pp. 376–394, 2016.

[11] M. Fabris And A. Pesci, "Automated Dem Extraction In Digital Aerial Photogrammetry: Precisions And Validation For Mass Movement Monitoring," *Ann. Geophys.*, Vol. 48, No. 6, 2005.

[12] V.-E. Oniga, A.-I. Breaban, And F. Statescu, "Determining The Optimum Number Of Ground Control Points For Obtaining High Precision Results Based On Uas Images," In *Multidisciplinary Digital Publishing Institute Proceedings*,

2018, Vol. 2, No. 7, P. 352.

[13] O. Eroglu, "Information Retrieval From Spaceborne Gnss Reflectometry Observations Using Physics-And Learning-Based Techniques," Electrical And Computer Engineering, 1986.

[14] G. J. J. Verhoeven, "It's All About The Format--Unleashing The Power Of Raw Aerial Photography," *Int. J. Remote Sens.*, Vol. 31, No. 8, Pp. 2009–2042, 2010.

[15] K. N. Tahar, "An Evaluation On Different Number Of Ground Control Points In Unmanned Aerial Vehicle Photogrammetric Block," *Int. Arch. Photogramm. Remote Sens. Spat. Inf. Sci*, Vol. 40, Pp. 93–98, 2013.

[16] M. V. Y. Garcia And H. C. De Oliveira, "The Influence Of Flight Configuration, Camera Calibration, And Ground Control Points For Digital Terrain Model And Orthomosaic Generation Using Unmanned Aerial Vehicles Imagery," *Bol. Ciências Geodésicas*, Vol. 27, 2021.

[17] B. Nagy, L. Kovács, And C. Benedek, "Sfm And Semantic Information Based Online Targetless Camera-Lidar Self-Calibration," In *2019 Ieee International Conference On Image Processing (Icip)*, 2019, Pp. 1317–1321.

[18] D. Suwardhi *Et Al.*, "3d Surveying, Modeling And Geo-Information System Of The New Campus Of Itb-Indonesia," *Int. Arch. Photogramm. Remote Sens. Spat. Inf. Sci.*, Vol. 42, P. 97, 2016.

[19] E. Husson, H. Reese, And F. Ecke, "Combining Spectral Data And A Dsm From Uas-Images For Improved Classification Of Non-Submerged Aquatic Vegetation," *Remote Sens.*, Vol. 9, No. 3, P. 247, 2017.

[20] B. Petzold, P. Reiss, And W. Stössel, "Laser Scanning—Surveying And Mapping Agencies Are Using A New Technique For The Derivation Of Digital Terrain Models," *Isprs J. Photogramm. Remote Sens.*, Vol. 54, No. 2–3, Pp. 95–104, 1999.